Spin dynamics of isolated donor electrons in phosphorus-doped silicon from high-frequency electron spin resonance

2010 J. Phys.: Condens. Matter 22 206001

(http://iopscience.iop.org/0953-8984/22/20/206001)

J. Phys.: Condens. Matter **22** (2010) 206001 (9pp) doi:10.1088/0953-8984/22/20/206001

Spin dynamics of isolated donor electrons in phosphorus-doped silicon from high-frequency electron spin resonance

Myeonghun Song[1], Minki Jeong[1], Byeongki Kang[1], Soonchil Lee[1], Tomohiro Ueno[2], Akira Matsubara[3], Takao Mizusaki[4,5,6], Yutaka Fujii[6], Seitaro Mitsudo[6] and Meiro Chiba[7,8]

[1] Department of Physics, Korea Advanced Institute of Science and Technology, Daejeon 305-701, Republic of Korea
[2] Graduate School of Medicine, Kyoto University, Kyoto 606-8501, Japan
[3] Research Center for Low Temperature and Materials Sciences, Kyoto University, Kyoto 606-8501, Japan
[4] Physics Department, Graduate School of Science, Kyoto University, Kyoto 606-8502, Japan
[5] Toyota Physical and Chemical Research Institute, Nagakute, Aichi 480-1192, Japan
[6] Research Center for Development of Far-Infrared Region, University of Fukui, Fukui 910-8507, Japan
[7] Graduate School of Engineering, University of Fukui, Fukui 910-8507, Japan
[8] Research Center for Quantum Computing, Interdisciplinary Graduate School of Science and Engineering, Kinki University, Higashi-Osaka 577-8502, Japan

E-mail: hunmsong@kaist.ac.kr

Received 22 February 2010, in final form 1 April 2010
Published 26 April 2010
Online at stacks.iop.org/JPhysCM/22/206001

Abstract

We present the spin dynamics of isolated donor electrons in phosphorus-doped silicon at low temperature and in a high magnetic field. We performed a steady-state electron spin resonance (ESR) on the sample with a dopant concentration of 6.5×10^{16} cm^{-3} in a high field of 2.87 T (80 GHz) and at temperatures from 48 down to 1.8 K. As the temperature decreases below 16 K, the resonance spectral line changes from the usual derivative form characteristic of absorptions. Very long spin–lattice relaxation time T_1 at low temperature gives rise to rapid passage effects and results in a dramatic change in the line shape and intensity as a function of temperature. We show that the numerical analysis based on the passage effects well explains the observed spectral changes with temperature. The spin–lattice relaxation time T_1 is derived by numerical fit to the experimental data. We discuss the dynamic nuclear polarization of ^{31}P nuclear spins which shows up as asymmetric intensities of the hyperfine-split ESR resonance lines.

1. Introduction

Many magnetic resonance studies from the 1950s to 1970s have been reported on the basic nature of phosphorus-doped silicon (Si:P), such as the metal–insulator transition with varying phosphorus donor concentration. Electron spin resonance (ESR) experiments on the donor electron spin have been performed extensively in a wide range of temperatures and external magnetic fields. Here we report the result of an ESR experiment performed under conditions of low temperature and high magnetic field not previously attempted. The original intent of this work was to obtain experimental evidence for, or against, the working principle of Kane's quantum computer model [1].

Among the various architectures that have been proposed to realize the quantum computation of many-qubits, the silicon-based nuclear spin system proposed by Kane has been pursued most intensively because of its compatibility for implementation with mature silicon technology. In Kane's model, ^{31}P nuclear spins located inside a silicon crystal with regular spaces are used as qubits. For a P nuclear spin to play the role of a qubit, the donor electron should be in the lowest energy level of the trapped donor states and the electron spins should be fully polarized. This requires temperatures lower

than 0.1 K and magnetic fields higher than 2 T, where the electron spins are more than 99% polarized.

Another requirement is that the nuclear spin coherence time or spin–spin relaxation time should be longer than the time necessary for a series of quantum gate operations. For the investigation of such nuclear spin dynamics, it is desirable to observe the nuclear magnetic resonance (NMR) of the isolated P nuclear spin in Si:P. NMR experiments have been carried out in a high field ($B = 7$ T) and at very low temperatures ($T < 0.1$ K) for highly doped Si:P, namely metallic samples [2, 3]. However, NMR experiments on isolated donor nuclear spin have never been reported because the NMR signal is too weak to be observed when the donor concentration is low enough for the ions to be isolated from each other. Instead of direct observation of the nuclear spin dynamics, ESR can be used to obtain information indirectly.

In this work, the isolated donor electron spin system is studied using steady-state ESR with field modulation at temperatures as low as 1.8 K and in a high magnetic field of 2.87 T. The observed spectral line shape and intensity changed drastically with temperature below 20 K. Since it is known that the electron spin–lattice relaxation time T_1 of P ESR for Si:P varies by several orders of magnitude with temperature [4, 5], we concluded that this drastic change of the spectrum is due to the variation of the passage conditions of the field modulation. We solved the Bloch equations numerically for various passage conditions to simulate the ESR spectrum and the result well explains the spectral changes. By comparison of the experimental data and calculation, we could derive T_1 in our experimental condition, which has not been observed.

At temperatures lower than 10 K, the intensities of the two hyperfine lines of the ESR spectra were slightly different, implying dynamic nuclear polarization (DNP) of ^{31}P nuclear spins [6]. We could induce up to 10% asymmetry in the lines by irradiating one of the lines with microwaves. Since this corresponds to the nuclear polarization enhancement of 10^3, direct observation of the NMR signal for the isolated donor nuclear spin system will be possible if DNP is adopted.

2. Experimental details

The high-frequency ESR experiment was performed at 80 GHz and at temperatures from 48 down to 1.8 K in a magnetic field of about 2.87 T. A block diagram of the experimental setup is shown in figure 1. The microwave source was a Gunn oscillator that was controlled by the phase-locked loop of a Millimeter-Wave Vector Network Analyzer (MVNA: ABmm). The microwave signal was measured by an InSb hot electron low-noise detector operating at 4.2 K. The signal was observed with the external field modulation of frequencies $\omega_m/2\pi = 330$ and 590 Hz and strength $B_m = 0.09$ mT through the lock-in output of the hot electron detector. A Si:P sample with a donor concentration of 6.5×10^{16} cm^{-3} was set inside the cylindrical waveguide. The size of the sample was $3 \times 3 \times 0.3$ mm^3. In order to observe the absorption signal, a simple transmission method was adopted without a cavity resonator. For the initial setup of the equipment, ESR spectra were taken for several different microwave frequencies around 80 GHz at 20 K in the slow passage condition. Then the operating frequency was chosen so as to observe only the absorption signal.

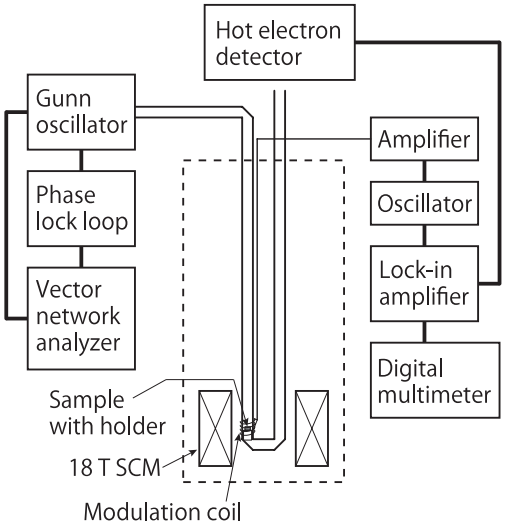

Figure 1. Block diagram of the high-frequency ESR apparatus. The microwave source is a Gunn oscillator that is phase-locked by a Millimeter-wave Vector Network Analyzer (MVNA: ABmm). The microwave signal is measured by an InSb hot electron detector operating at 4.2 K. The coil for the field modulation is wound on the cylindrical waveguide near the sample.

3. Results

The electron spin Hamiltonian describing the system of an isolated trapped donor in a magnetic field $\boldsymbol{B}$ applied along the z axis is

$$\mathcal{H} = g\mu_B B S_z + A\boldsymbol{I}\cdot\boldsymbol{S}, \tag{1}$$

where μ_B is the Bohr magneton and A the hyperfine coupling energy. Here $\boldsymbol{S}$ and $\boldsymbol{I}$ are the electron spin and the ^{31}P nuclear spin, respectively, where $S = \frac{1}{2}$ and $I = \frac{1}{2}$. Since the donor electron behaves like the s-state in the hydrogen atom centered at the P^+ ion, there is no orbital moment causing g-shift and therefore, $g = 2$. The resonance frequencies are then given by

$$\omega_{res} = \frac{g\mu_B}{\hbar}\left(B \pm \frac{1}{2}\frac{A}{g\mu_B}\right). \tag{2}$$

The ESR spectrum of the isolated P ion spin has two lines separated by $A/g\mu_B$, which is known to be 4.2 mT [7]. One line comes from the electron spin tied with an 'up' nuclear spin, and the other from a 'down' nuclear spin. Hereafter the resonance line appearing at the higher field is referred to as the H-line and the one at the lower field is referred to as the L-line.

The ESR spectra of Si:P obtained at $\omega_m/2\pi = 330$ Hz and various temperatures are plotted in figure 2. The audio-frequency phase for the field modulation was adjusted in such a way that only the in-phase signal but not the 90° out-of-phase signal (hereafter referred to as the *out-of-phase signal*) is observed for $T > 16$ K, because this is the temperature region satisfying the slow passage condition and it is well known that the out-of-phase signal is unobservable in that condition. The

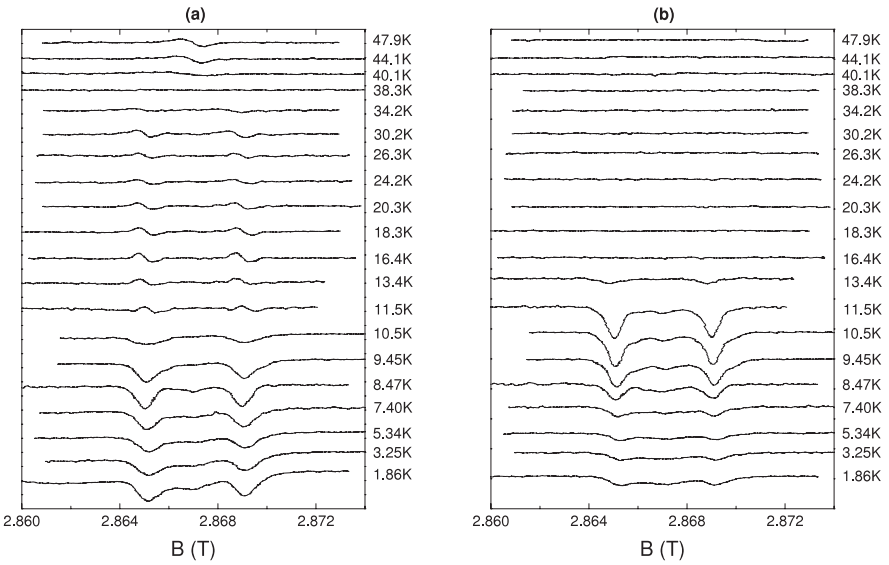

Figure 2. Temperature dependence of ESR spectrum of Si:P (6.5×10^{16} cm^{-3}). The microwave frequency is 80 GHz and the field modulation frequency is 330 Hz. (a) and (b) are, respectively, the in-phase and out-of-phase signals with respect to the reference phase of the modulation.

in-phase and out-of-phase signals are shown in figures 2(a) and (b), respectively. Both signals clearly show two peaks at most of the measured temperatures, named above as the H- and L-lines.

These two spectral lines become broad with increasing temperature and finally disappear around 38 K. With further increasing of temperature a single line appears. This is the effect of the motional narrowing. Thermally activated trapped electrons in the conduction band hop from one site to another. If the inverse of the hopping time $1/\tau$ becomes larger than the angular frequency of the splitting of the two hyperfine lines, the lines merge to a single narrow line by the motional narrowing. Let us compare the observed spectrum in figure 2 with the spectrum in figure X,2 in the textbook by Abragam [8]. In the case of Si:P, the hyperfine splitting is 4.2 mT which corresponds to $2\delta \simeq 7 \times 10^8$ rad s^{-1}. Referring to the figure in the textbook, the observed signals at 30.2, 34.2, 40.1, and 47.9 K correspond, respectively, to $4\delta\tau = 100$, 10, 1, and 10^{-2}. Then the corresponding hopping times are found to be $\tau = 7 \times 10^{-8}$, 7×10^{-9}, 7×10^{-10}, and 7×10^{-12} s.

In the temperature region between 16 and 30 K (region III), the line shape of the in-phase signal is an odd function representing the derivative of the absorption line. This is the line shape usually observed in ESR experiments using field modulation satisfying the slow passage condition. By contrast, in the temperature region below 11 K (region I), both the in-phase and out-of-phase line shapes are even functions. Temperature region II between 11 and 16 K is the transition region. The in-phase signal is the mixture of even and odd functions but the out-of-phase signal is purely even. Since the out-of-phase signal is unobservable in the slow passage condition, its appearance in regions I and II below 16 K means that the slow passage condition is broken there. It is worth noting that the out-of-phase signals are always even.

The temperature dependence of the signal intensity $I_{\rm exp}(T)$ is plotted in figure 3, together with the temperature regions defined above and the typical in-phase signal shape of each region. Region II is the temperature region below 16 K where the out-of-phase signal starts to appear, and above 11 K where it reaches a maximum. Intensities of the in-phase signal were measured by the peak-to-peak values in region III, the peak-to-peak or peak height in II, and by the peak heights in I as shown by the arrows in the figure. Intensities of the out-of-phase signal were measured by the peak height. The intensity is normalized by the Brillouin function with a magnetic field of 2.87 T and $S = 1/2$ to be compared later with the result of numerical calculation.

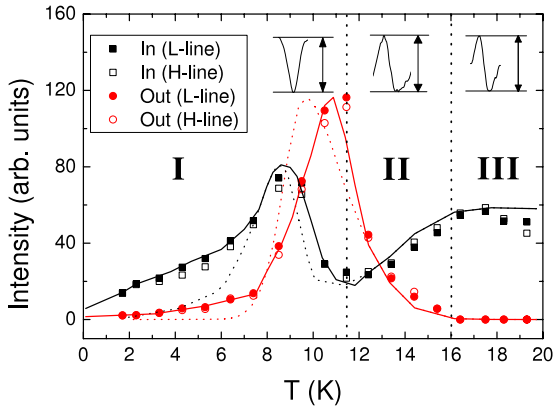

Figure 3. Temperature dependence of the normalized ESR signal intensity $I_{\rm exp}(T)$ and the typical in-phase signal shapes for Si:P. Modulation frequency is 330 Hz. Intensity is defined as the length of the double-ended arrows in the figure. The square symbols represent the signal intensity of the in-phase signals and the circles represent the out-of-phase signals. The solid and open symbols are the intensities of the L- and H-lines, respectively. The lines are the results of the numerical calculation of the Bloch equations (see section 4.3).

(This figure is in colour only in the electronic version)

When the distance between the trapped donor ions is not much larger than their Bohr radius, the exchange interaction

generates metallic P clusters of various sizes. The ESR spectrum of the clusters is found at the center of the H- and L-lines [9], because the directions of the nuclear spins interacting with an electron spin are averaged out. The trace of such a center peak is also found at low temperatures in figure 2. The out-of-phase signals became very small in region I. The cluster signal continued to grow as temperature decreased and became comparable to the isolated donor signal below 6 K. At these temperatures the out-of-phase signal heights were measured after subtracting the average height of the cluster signal from the peak intensity at $\omega = \omega_{\rm res}$. Below 6 K, a very broad background signal was also observed in the in-phase signals, which may result from tiny residue of the powdered 1,1-Diphenyl-2-picrylhydrazyl (DPPH) test sample. We measured the signal intensity of the background outside of the H- and L-lines and used it to correct the signal.

It is noticed that the intensity of the L-line is always slightly larger than that of the H-line at temperatures below 10 K by about 10% at most. In the experiment, ESR data were taken by sweeping a field back and forth between the L-line and H-line at a 30 min interval. This asymmetry of 10% will be ignored in the following discussions until the DNP effect on ^{31}P nuclear spins is discussed in section 5.

4. Passage condition and spectral change

Here we consider the dynamics of the spin packets producing broad inhomogeneous spectral lines. Each resonance line has inhomogeneous broadening of about 0.25 mT [10] due to the hyperfine interaction with randomly distributed ^{29}Si nuclear spins ($I = 1/2$) with an abundance of 4.7%. The broadened line shape function, $h(\omega, \omega_{\rm res})$, is centered at $\omega_{\rm res}$ given by equation (2) and composed of the wavepackets centered at their own resonance frequency ω. Phenomenologically, the spins generating each wavepacket follow the Bloch equations,

$$\begin{aligned}\frac{{\rm d}M_x}{{\rm d}t} &= -\gamma b_z M_y - \frac{M_x}{T_2}\\ \frac{{\rm d}M_y}{{\rm d}t} &= \gamma b_z M_x - \gamma B_1 M_z - \frac{M_y}{T_2}\\ \frac{{\rm d}M_z}{{\rm d}t} &= \gamma B_1 M_y + \frac{M_0 - M_z}{T_1},\end{aligned} \tag{3}$$

in the frame rotating around the z axis with the angular frequency $\omega = B_0/\gamma$, when the direction of magnetic field $B_0 + b_z$ is parallel with the z axis in the laboratory frame. Here, $\gamma = g\mu_{\rm B}/\hbar$ is the gyromagnetic ratio and M_α is the α component of magnetization $\boldsymbol{M}$. The residual magnetic field b_z is the deviation from the resonance field and B_1 the radiofrequency (rf) magnetic field along the x axis direction. In an experiment where a magnetic field modulation along the z axis is used, another term is added to b_z as,

$$b_z = \frac{\delta\omega}{\gamma} + B_{\rm m}\cos\omega_{\rm m}t, \tag{4}$$

where $\delta\omega/\gamma$ is the deviation of an applied field B from the resonance field B_0. $B_{\rm m}$ and $\omega_{\rm m}$ are the amplitude and the angular frequency of the field modulation, respectively.

4.1. Passage condition

The effect of the passage condition on the observed spectral line shape has been discussed, for example by Portis [11], Weger [12], and Chiba *et al* [13]. Here we give a rough sketch of the passage effect based on their discussion and provide an introduction to the numerical solution of the Bloch equations discussed in section 4.2.

Three important parameters, which specify various passage conditions, are defined as,

$$\varepsilon_{\rm A} = \frac{\gamma B_1^2}{B_{\rm m}\omega_{\rm m}} \qquad \varepsilon_{\rm R} = \frac{B_{\rm m}}{B_1}\,\omega_{\rm m}T_1 \qquad \varepsilon_{\rm F} = \omega_{\rm m}T_1. \tag{5}$$

These parameters have the following meanings:

(1) The *adiabatic* passage condition for $\varepsilon_{\rm A} \gg 1$ is satisfied when angular velocity

$$\Omega = \frac{1}{B_1}\frac{{\rm d}b_z}{{\rm d}t} \tag{6}$$

of the effective field

$$\boldsymbol{B}_{\rm eff} = b_z\boldsymbol{k} + B_1\boldsymbol{i}, \tag{7}$$

where $\boldsymbol{k}$ and $\boldsymbol{i}$ are the unit vectors along the z and x axes in the rotating frame of reference, respectively, is much smaller than the Larmor angular frequency $\gamma B_{\rm eff}$. Here, the adiabatic condition is most severe when the applied field passes through the resonance field. Then from equation (4), the adiabatic condition is given as $\gamma B_1 \gg \Omega\,(=B_{\rm m}\omega_{\rm m}/B_1)$. This is equivalent to the condition of $\varepsilon_{\rm A} \gg 1$. In the present experimental condition, $B_1 \sim 10^{-3}$ mT, $B_{\rm m} \sim 0.1$ mT and $\omega_{\rm m} \sim 2\times10^3$ rad s^{-1}, and $\varepsilon_{\rm A}$ is of the order of unity. The experimental condition was not fully adiabatic but *quasi-adiabatic*.

(2) The *rapid* passage condition for $\varepsilon_{\rm R} \gg 1$ is satisfied if the time for the external field to pass through the resonance region (resonance field $\pm$ microwave field B_1) is much shorter than T_1. This leads us to $\varepsilon_{\rm R} \gg 1$.

(3) The *fast* passage condition for $\varepsilon_{\rm F} \gg 1$ is satisfied when the modulation period is much shorter than T_1. *Rapid* and *fast* are the terms used by Weger [12]. Here $\varepsilon_{\rm A}$ is temperature independent and $\varepsilon_{\rm R} \gg \varepsilon_{\rm F}$ because $B_{\rm m} \gg B_1$ in this experiment. We call the condition for $\varepsilon_{\rm R} \ll 1$ the slow passage, following the convention, and refer to the condition for $\varepsilon_{\rm F} \ll 1$ the non-fast passage.

Portis [11] has proposed the following formula to include the onset of the rapid passage effect when $\varepsilon_{\rm R}$ is still much smaller than one,

$$\{\chi'(\omega)\}_{\text{linear in }\varepsilon_{\rm R}} = \frac{\pi}{4}\chi_0\,\omega\varepsilon_{\rm R}\cos\phi\; h(\omega,\omega_{\rm res})\sin(\omega_{\rm m}t - \phi), \tag{8}$$

where χ_0 is the static susceptibility, ω/γ the external magnetic field, and $\phi = \tan^{-1}(\omega_{\rm m}T_1)$. The dispersion signal χ' is expressed as a power series expansion of $\varepsilon_{\rm R}$. The function $h(\omega, \omega_{\rm res})$ is the inhomogeneous line distribution function defined in the beginning of this section. At the onset of the rapid passage $\phi \simeq \varepsilon_{\rm R} \ll 1$, the motion of M_x appears in

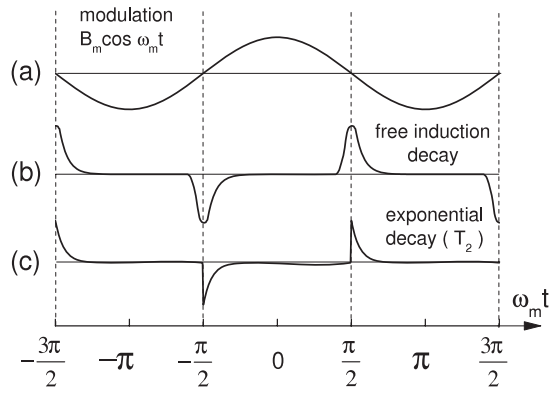

Figure 4. Timing chart of the modulation field and signal: (a) cosine wave of magnetic field modulation; (b) free induction decay after sudden passage; (c) simplified model of exponential decay with a time constant of T_2.

the out-of-phase signal. This fact is related to the reason why the out-of-phase signal appeared only below 16 K in the experiment. Equation (8) points out that the line shape of the M_x signal is determined by $h(\omega, \omega_{\rm res})$ while that of the M_y signal is given by the derivative of $h(\omega, \omega_{\rm res})$. However, it should be noted that this anomalous behavior in the ESR spectrum appears in the dispersion signal, $M_x(\omega)$.

Here we consider the spin dynamics for the case where $\varepsilon_{\rm R} \gg 1$ (the rapid passage), $\varepsilon_{\rm F} \ll 1$ (the non-fast condition), and $\varepsilon_{\rm A} \simeq 1$ (the quasi-adiabatic passage). Since the motion of a spin follows the rapid passage, it is better to treat the magnetization M rather than the susceptibility χ. The timing chart of the modulation field is shown in figure 4. A cosine magnetic field modulation given by equation (4) for $\delta\omega = 0$ is depicted in figure 4(a), where the vertical lines indicate the moments when the spin packets are just in resonance. $M_x(t)$, shown in figure 4(b), appears at the moments of resonance, and then decays with the time constant T_2 when $\omega_{\rm m} T_2 \ll 1$. In this experiment, $T_2 \leqslant 10^{-4}$ s and thus $\omega_{\rm m} T_2 < 1$. For ease of calculation, the decay function was simplified to an exponential function with the decay time constant T_2. The lock-in output signal S is proportional to the Fourier component of $M_x(t)$ at $\omega_{\rm m}$ and given by the integration over one period as

$$\begin{aligned} S &= \frac{1}{2\pi/\omega_{\rm m}} \int_{-\pi/2\omega_{\rm m}}^{3\pi/2\omega_{\rm m}} M_x(t) \exp(\mathrm{i}\omega_{\rm m} t)\, \mathrm{d}t \\ &= -\frac{|M_x(0)|}{\pi} (\omega_{\rm m} T_2) \frac{1 + \mathrm{e}^{-\pi/\omega_{\rm m} T_2}}{1 + (\omega_{\rm m} T_2)^2} (\omega_{\rm m} T_2 - \mathrm{i}). \end{aligned} \tag{9}$$

The in-phase and out-of-phase signals of the lock-in detection, $M_x^{\rm IN}$ and $M_x^{\rm OUT}$, correspond to the real and imaginary parts of S, respectively. It should be noted that $M_x^{\rm IN}$ increases as $(\omega_{\rm m} T_2)^2$ and therefore $M_x^{\rm OUT}$ is much bigger than $M_x^{\rm IN}$ for $\omega_{\rm m} T_2 \ll 1$.

When $\varepsilon_{\rm R} \gg 1$ and $\varepsilon_{\rm F} \ll 1$, $M_x(0)$ is approximately given by

$$M_x(0) \simeq M_0 \simeq \chi_0 B, \tag{10}$$

and the shift of the phase ϕ is given by,

$$\phi = \tan^{-1}(-\omega_{\rm m} T_2). \tag{11}$$

If $T_2 = T_1$ (the motional narrowing case at high temperature), these equations are reduced to a formula similar to Portis's equation (equation (8)).

4.2. Numerical calculation of the Bloch equations

The numerical calculations of the Bloch equations are carried out to simulate the lock-in output of $M_\alpha^{\rm IN}(\omega - \omega_{\rm res})$ and $M_\alpha^{\rm OUT}(\omega - \omega_{\rm res})$ in three steps.

(1) First, we explicitly solved the Bloch equations in equation (3) for the spin packets rotating with ω by using the GNU Scientific Library to obtain the time evolution of $M(t)$ for a given $\delta\omega$ defined by equation (4). The frequency range of $\delta\omega$ was set to $\pm 6\gamma B_{\rm m}$ so as to cover the long tail of the Lorentzian function with the width, $1/T_2$.

(2) After steady-state solutions were obtained at $t > 5T_1$, their time averages over the period of the field modulation $2\pi/\omega_{\rm m}$ were calculated for various T_1 and $\delta\omega$ as,

$$\begin{aligned} &\overline{M_\alpha \cos \omega_{\rm m} t}(\delta\omega, T_1) \\ &\quad \equiv \frac{\omega_{\rm m}}{2\pi} \int_0^{2\pi/\omega_{\rm m}} M_\alpha(t, \delta\omega, T_1) \cos \omega_{\rm m} t\, \mathrm{d}t, \end{aligned} \tag{12}$$

where $\alpha = x, y$. The cosine component corresponds to the in-phase signal of the lock-in detector. The out-of-phase signal is calculated by multiplying $\sin \omega_{\rm m} t$ by M_α.

(3) The convolutions of the response function, equation (12), of the spin packets with $h(\omega, \omega_{\rm res})$ are calculated to obtain $M_\alpha^{\rm IN}(\omega - \omega_{\rm res})$ and $M_\alpha^{\rm OUT}(\omega - \omega_{\rm res})$ as

$$M_\alpha^{\rm IN}(\omega - \omega_{\rm res}) = \int_{-\infty}^{\infty} \overline{M_\alpha \cos \omega_{\rm m} t}(\omega' - \omega) h(\omega', \omega_{\rm res})\, \mathrm{d}\omega', \tag{13}$$

and

$$M_\alpha^{\rm OUT}(\omega - \omega_{\rm res}) = \int_{-\infty}^{\infty} \overline{M_\alpha \sin \omega_{\rm m} t}(\omega' - \omega) h(\omega', \omega_{\rm res})\, \mathrm{d}\omega'. \tag{14}$$

The values of the parameters used in the calculation are $\omega_{\rm m}/2\pi = 330$ Hz ($\omega_{\rm m} = 2.1 \times 10^3$ rad s^{-1}), $B_{\rm m} = 9.1 \times 10^{-5}$ T ($\gamma B_{\rm m} = 1.6 \times 10^7$ rad s^{-1}), and $B_1 = 1.1 \times 10^{-6}$ T ($\gamma B_1 = 2.0 \times 10^5$ rad s^{-1}). The inhomogeneously broadened line spectrum $h(\omega, \omega_{\rm res})$ is given by a Gaussian shape distribution function,

$$h(\omega, \omega_{\rm res}) = \frac{1}{\sqrt{2\pi}\sigma} \exp\left(-\frac{(\omega - \omega_{\rm res})^2}{2\sigma^2}\right), \tag{15}$$

where σ is the width of the distribution. We determined σ for this sample by fitting the spectrum in the slow passage region around 16 K and the result is $\sigma = 6.2 \times 10^7$ rad s^{-1} ($\sigma/\gamma = 0.35$ mT).

The spin–spin relaxation time T_2 has been measured by the spin echo decay time in the X-band pulse ESR [14, 15]. The relaxation rate $1/T_2$ at low temperature is determined by the rigid-lattice value of the electron–^{29}Si nuclear dipole interaction that is independent of temperature and field. Following these previous ESR studies, we chose $T_2 = T_1$, the condition satisfied in the motional narrowing limit, if $T_1 < 10^{-4}$ s, and $T_2 = 10^{-4}$ s, the rigid-lattice value independent of

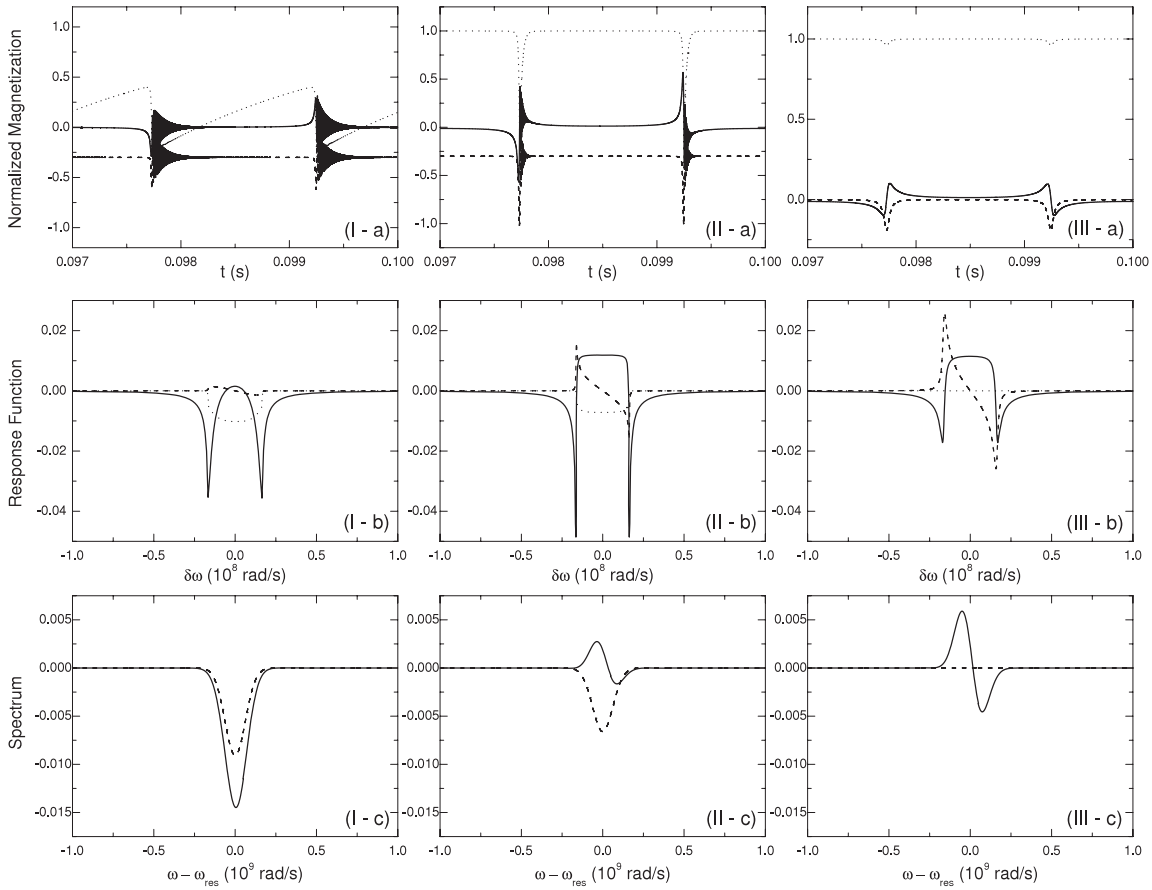

Figure 5. Numerical calculation of the Bloch equations. Column I is the result for region I ($T_1 = 2 \times 10^{-3}$ s and $T_2 = 10^{-4}$ s), column II for region II ($T_1 = T_2 = 5 \times 10^{-5}$ s) and column III for region III ($T_1 = T_2 = 10^{-6}$ s). Row (a) shows results for the time evolutions of $M_\alpha(t)$ after $t > 5T_1$ at $\delta\omega = 0$. Solid lines show $\overline{M_x(t)}$, dashed lines $M_y(t)$, and dotted lines $M_z(t)$. In (I-a) and (II-a), $M_x(t)$ is vertically shifted by -0.3 to clarify the figure. Row (b) shows $\overline{M_x \cos\omega_m t}$ (solid line), $\overline{M_x \sin\omega_m t}$ (dotted line), and $\overline{M_y \cos\omega_m t}$ (dashed line) as functions of $\delta\omega$ for the regions I, II, and III, respectively. Row (c) shows $M_x^{\rm IN} + 3.5M_y^{\rm IN}$ (solid line) and $M_x^{\rm OUT}$ (dashed line).

T, if $T_1 \geqslant 10^{-4}$ s. It should be noted that the inhomogeneous line width ($\sim 6.2 \times 10^7$ rad s^{-1}) is much larger than the line width of the Bloch equations ($2\pi/T_2 \sim 6 \times 10^4$ rad s^{-1}) and thus the wavepacket approximation is valid. Now the only parameter left unknown in the Bloch equations is T_1 and therefore it is solved numerically as a function of T_1. The temperature dependence of the ESR spectrum is attributed to the temperature dependence of $T_1(T)$ since T_2 is fixed at 10^{-4} s for most temperature regions of the experiment.

$M(t)$ was normalized by its value at $t = 0$ so that the numerical solutions for $M_\alpha^{\rm IN}$ and $M_\alpha^{\rm OUT}$ could be compared with the experimental results normalized by the Brillouin function for $B = 2.87$ T and $S = 1/2$. The calculation usually starts from the initial condition, $(M_x, M_y, M_z) = (0, 0, 1)$ and then the magnetization continues the time evolution until it reaches the steady-state solution at $t > 5T_1$. In fact, the solution was almost independent of the initial condition.

Figure 5 shows the typical results of the simulations for three different temperature regions. The results were obtained with $T_1 = 2 \times 10^{-3}$ s and $T_2 = 10^{-4}$ s in region I, $T_1 = T_2 = 5 \times 10^{-5}$ s in region II, and $T_1 = T_2 = 10^{-6}$ s in region III. Region I is the region of the rapid and fast passage condition ($\varepsilon_{\rm R} \gg 1$ and $\varepsilon_{\rm F} \gg 1$), region II the rapid and non-fast passage condition ($\varepsilon_{\rm R} \gg 1$ and $\varepsilon_{\rm F} \ll 1$), and region III the slow and non-fast passage condition ($\varepsilon_{\rm R} \ll 1$ and $\varepsilon_{\rm F} \ll 1$).

Figures 5(I-a), (II-a), and (III-a) show the steady-state time evolutions of $M(t)$ at $\delta\omega = 0$ for the three passage conditions. In the cases of I and II where the rapid passage condition $\varepsilon_{\rm R} \gg 1$ is met, $M(t)$ rotates almost together with the instantaneous effective field $B_{\rm eff}$ when the sweep field of modulation goes through the resonance point within $\pm B_1$, as shown schematically in figure 4(b). Since $\varepsilon_{\rm A} \simeq 1$, the spin motion does not exactly follow the adiabatic rapid passage, that is, M_z is not completely reversed and a finite M_x remains after the passage through the resonance point within $\pm B_1$. It should be noted, however, that $M_y \ll M_x$ for $\varepsilon_{\rm R} \gg 1$. After the sweep field passes through the resonance point, $M_x(t)$ decays with T_2 together with a ringing signal at an instantaneous local frequency, γb_z, given by equation (4). After the ringing dies out, a finite $M_x(t)$ remains, which is locked to the B_1-field in the rotating frame of reference and thus shows no ringing. The difference between (I) and (II) is that $\varepsilon_{\rm F} \gg 1$ (fast) in (I) while $\varepsilon_{\rm F} \ll 1$ (non-fast) in (II). Therefore, M_z recovers during each cycle of the field sweep in (II) but not in (I). In the slow passage condition (III-a), the time constants T_1 and T_2 are so short that $M_\alpha(t)$ ($\alpha = x, y, z$) traces the instantaneous equilibrium value

(steady-state solution for the Bloch equations) at any instance during the field sweep.

Figures 5(I-b), (II-b), and (III-b) show the response functions to the Bloch equations, $\overline{M_x \cos\omega_m t}(\delta\omega, T_1)$ (solid curves), $\overline{M_x \sin\omega_m t}(\delta\omega, T_1)$ (dotted curves), and $\overline{M_y \cos\omega_m t}$ $(\delta\omega, T_1)$ (dashed curves), calculated by equation (12) in each region. It is worth noting that in all cases, $\overline{M_x \cos\omega_m t}$ and $\overline{M_x \sin\omega_m t}$ are even functions for $\delta\omega$ and $\overline{M_y \cos\omega_m t}$ is an odd function. Since $\overline{M_y \sin\omega_m t}$ is negligibly small in all the T_1 range it is not shown. In region III, $\overline{M_y \cos\omega_m t}$ is a main signal and $\overline{M_x \cos\omega_m t}$ is not small. However, $\overline{M_x \sin\omega_m t}$ is much smaller than the others because in the slow passage region, M responds to the field modulation without a delay. In region II, $\overline{M_x \sin\omega_m t}$ starts to grow as predicted in section 4.1. $\overline{M_y \cos\omega_m t}$ and $\overline{M_x \cos\omega_m t}$ are comparable to each other and therefore the in-phase signal is composed of the absorption and dispersion signals. In region I, $\overline{M_y \cos\omega_m t}$ is very small and the main signal is produced by $\overline{M_x \cos\omega_m t}$ and $\overline{M_x \sin\omega_m t}$. This is the reason why the line shapes of both the in-phase and out-of-phase signals are even functions in region I.

Once $\overline{M_\alpha \cos\omega_m t}$ and $\overline{M_\alpha \sin\omega_m t}$ are obtained, the observed in-phase signal $M_\alpha^{\rm IN}(\omega - \omega_{\rm res})$ and out-of-phase signal $M_\alpha^{\rm OUT}(\omega - \omega_{\rm res})$ are calculated by equation (13) and equation (14), respectively. Since the value of the convolution of an odd function is much smaller than that of an even function, $M_y^{\rm IN}$ was multiplied by 3.5, which gives the best fit to the experimental data. Figures 5(I-c), (II-c), and (III-c) show the in-phase signals $M^{\rm IN} \equiv M_x^{\rm IN}(\omega-\omega_{\rm res})+3.5M_y^{\rm IN}(\omega-\omega_{\rm res})$ (solid curves) and out-of-phase signals $M^{\rm OUT} \equiv M_x^{\rm OUT}(\omega - \omega_{\rm res})$ (dashed curves). In region III, $M^{\rm IN}$ is almost an odd function which is the derivative of $h(\omega, \omega_{\rm res})$ because the main contribution, $\overline{M_y \cos\omega_m t}$, to the in-phase signal is odd. In region I, $M^{\rm IN}$ is an even function, $h(\omega, \omega_{\rm res})$ itself, because $\overline{M_x \cos\omega_m t}$ is even. In region II, $M^{\rm IN}$ is a mixture of even and odd functions. However, $M^{\rm OUT}$ is always an even function because the out-of-phase signal comes from only $\overline{M_x \sin\omega_m t}$, which is even. Row (c) in figure 5 shows well how the line shapes change as the passage condition varies with T_1.

In figure 6, T_1 dependence of the signal intensities $I_{\rm cal}(T_1)$ obtained from $M^{\rm IN}$ and $M^{\rm OUT}$ are shown. The intensities of $M^{\rm IN}$ s were obtained by peak-to-peak values in region III, peak heights in region I and peak-to-peak values or peak heights in region II while those of $M^{\rm OUT}$s were obtained by peak heights in all regions. The vertical dotted lines indicate the points where $\varepsilon_{\rm F} = 1$ and $\varepsilon_{\rm R} = 1$. $\sqrt{M^{\rm IN}(T_1)^2 + M^{\rm OUT}(T_1)^2}$ reaches the maximum and $M^{\rm IN}(T_1) \approx \frac{1}{2}M^{\rm IN}(\varepsilon_{\rm R} \ll 1)$ near the points where $\varepsilon_{\rm F} = 1$ and $\varepsilon_{\rm R} = 1$, respectively.

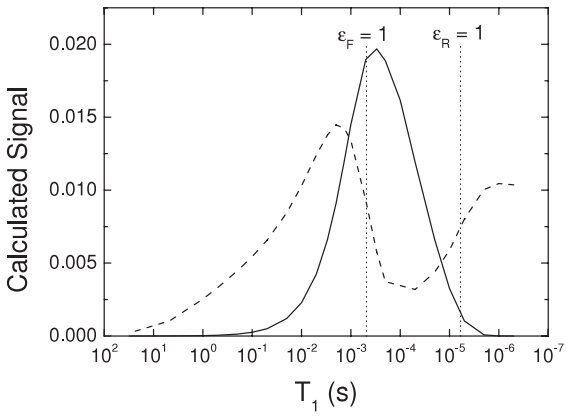

Figure 6. T_1 dependence of calculated signal intensities $I_{\rm cal}(T_1)$. The solid line represents the out-of-phase intensity obtained from $M^{\rm OUT}$. The dashed line represents the in-phase intensity from $M^{\rm IN}$. The vertical dotted lines indicate the points where $\varepsilon_{\rm F} = 1$ and $\varepsilon_{\rm R} = 1$.

4.3. Simulation

Now we can simulate the experimental observation $I_{\rm exp}(T)$ with the result of the numerical calculation $I_{\rm cal}(T_1)$ to understand the change of the spectral line shape and intensity with temperature, if the temperature dependence of the spin–lattice relaxation time $T_1(T)$ is given. In general, the unknown parameter T_1 is a function of temperature, field, and doping concentration in ESR for Si:P. Although T_1 has not been measured in our experimental condition of $B = 2.87$ T and $n = 6.52 \times 10^{16}$ cm^{-3}, it can be guessed from previous works. Feher and Gere [4] pointed out that T_1 is strongly dependent on concentration above $n = 10^{16}$ cm^{-3} but constant below that at low temperature. They also presented the temperature dependence of T_1 measured below 4.2 K and at $B = 0.3$–0.8 T for $n = 7 \times 10^{16}$ cm^{-3}, which is quite close to the concentration of our sample. The observed T_1 is independent of magnetic field from 0.3 to 0.8 T and well explained by the exchange coupling between the neighboring phosphorus donors [16]. At high temperatures above 6 K, the main mechanism of T_1 relaxation is the Orbach process [17], where T_1 is almost independent of concentration and field. The relaxation rate $1/T_1$ is proportional to $e^{-\Delta/kT}$, where Δ is the energy difference between the ground state and the first excited state lifted by valley–orbit coupling [18]. The measured values of T_1 at $B = 0.17$–0.33 T for $n = 0.9$–1.7×10^{16} cm^{-3} were presented by Castner [19] and Tyryshkin *et al* [15]. Their values are consistent with each other and independent of concentration and field as expected. The temperature dependencies of the observed T_1 due to the phosphorus–phosphorus exchange (P–P exchange) interaction and Orbach process are shown together in figure 7 (thin solid line). Considering the fact that T_1 relaxation due to the P–P exchange interaction has no dependence on magnetic field, and that due to the Orbach process is independent of concentration, we may take the thin solid line in the graph to simulate the spectrum expected in our experimental condition.

With $T_1(T)$ obtained from the thin solid line and $I_{\rm cal}(T_1)$, we can estimate $I_{\rm cal}(T)$. In figure 3, the calculated value $I_{\rm cal}(T)$ (dotted lines) is shown together with the experimental value $I_{\rm exp}(T)$. The numerical result qualitatively well follows the complicated temperature dependence of the experimental data in the whole temperature range of the experiment. Quantitatively, $I_{\rm cal}(T)$ is well fitted to $I_{\rm exp}(T)$ at temperatures above 11 K, while it is poorly matched with $I_{\rm exp}(T)$ at temperatures below 8 K. This means that the relaxation time adopted for the simulation is far from the real value at low temperature. Therefore, we took the inverse process, that is we derived the real relaxation times that make the calculation

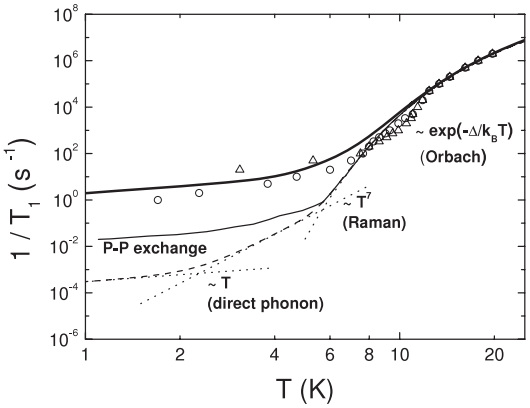

Figure 7. Temperature dependence of the spin–lattice relaxation rate $1/T_1$ reported in the literature: the dashed lines are from Feher and Gere [4], Castner [19] and Tyryshkin *et al* [15]. The thin solid line is the data used for the initial simulation and the thick solid line is the theoretical prediction of equation (16) for $B = 2.87$ T and $n = 6.52 \times 10^{16}$ cm^{-3}. The open circles (triangles) represent the $1/T_1$ values derived by comparison of the in-phase (out-of-phase) signal intensities of $I_{\rm cal}(T_1)$ and $I_{\rm exp}(T)$.

result fit best to the data. The values obtained in this way are shown in figure 7 by open symbols. The open circles (triangles) represent the $1/T_1$ values derived by comparison of the in-phase (out-of-phase) signal intensities of $I_{\rm cal}(T_1)$ and $I_{\rm exp}(T)$. The relaxation rate determined in our experiment is well explained by the Orbach process at high temperature, but is larger than the value expected in the P–P exchange interaction by two orders of magnitude at low temperature. The spectral intensity predicted by these relaxation rates is shown as the solid lines in figure 3.

Feher and Gere [4] reported also T_1 observed at $B = 0.32$ T and $T < 4.2$ K for a sample with its concentration lower than $n = 10^{16}$ cm^{-3}, below which the relaxation time is independent of concentration (dashed line in figure 7). In this concentration range, the main mechanism of T_1 relaxation is the direct phonon process for $T < 2.5$ T and the Raman process for $T > 2.5$ T. Both processes are dependent on magnetic field and the empirical formula [5] giving the total relaxation rate as

$$\frac{1}{T_1} = aB^4T + bB^2T^7 + c\exp\left(-\frac{\Delta}{k_{\rm B}T}\right), \qquad (16)$$

where the first term describes the direct phonon process, the second term the Raman, and the last term the Orbach. The dashed line fits to equation (16) with the fitting parameters, $a = 2.86 \times 10^{-2}$ s^{-1} T^{-4} K^{-1}, $b = 1.95 \times 10^{-5}$ s^{-1} T^{-2} K^{-1}, $c = 0.91 \times 10^{9}$ s^{-1} and $\Delta/k_{\rm B} = 122.5$ K. With these fitting parameters, we tried to estimate the relaxation rate expected at 2.87 T, the field of our experiment. The theoretical result shown in figure 7 by a thick solid line matches excellently with our experimental data. It is clear that the T_1 relaxation process at low temperature is determined by the phonon process at 2.87 T. The P–P exchange interaction is dominant at low field but the relaxation due to the phonon process surpasses that due to the P–P exchange interaction around 1 T.

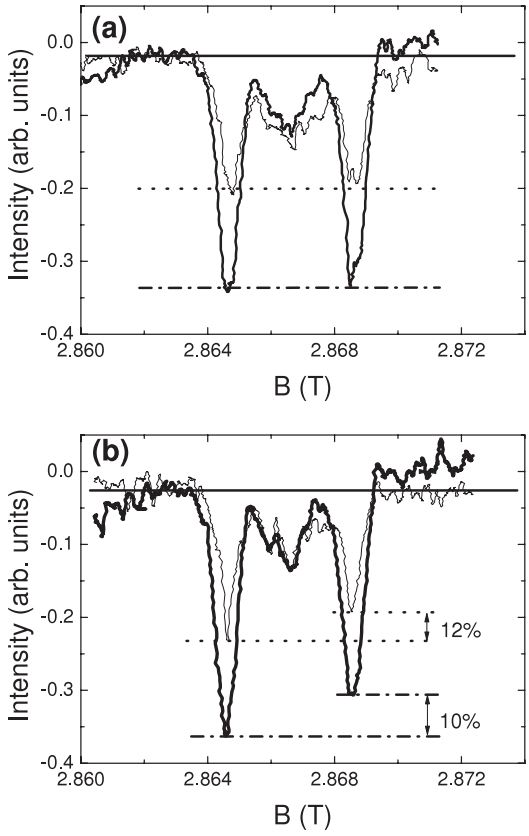

Figure 8. ESR spectra for Si:P at 6.9 K. Spectra (a) before and (b) after microwave irradiation for 20 min.

5. Dynamic nuclear polarization

Figure 3 shows that the intensity of the H-line (open symbols) is a little smaller than that of the L-line (solid symbols). This asymmetry of the two lines become significant below about 10 K. Present ESR data were taken by sweeping a magnetic field back and forth between the L- and H-lines every 30 min under continuous microwave irradiation. Since the L-line corresponds to the state $\left|I = \frac{1}{2}\right\rangle$ of a ^{31}P nuclear spin and the H-line to the state $\left|I = -\frac{1}{2}\right\rangle$, we suggest that this asymmetry of the two lines is due to the DNP effect. In fact, the DNP has already been observed in Si:P at the applied field of 0.32 T [20, 21]. It has been discussed as resulting from the shift of the spectral line of the cluster [22], and the DNP effect by irradiation of visible light has also been recently reported [23].

In order to confirm our guess, the intensities of the resonance signals obtained before and after microwave radiation were compared. The result observed just after cooling from the high temperature of 70 down to 6.9 K is shown in figure 8(a). Here the external field was swept downward from the H- to L-lines. The in-phase signal is shown by the thick-line curve and the out-of-phase signal is shown by the thin-line curve. Both the in-phase and out-of-phase signals show that the intensities of the L- and H-lines are almost equal. Next, the H-line was subjected to microwave irradiation for 20 min. The ESR spectrum observed just after irradiation is shown in figure 8(b). The intensity of both the in-phase and out-of-phase signals in the L-line is about 10% larger than that in the

H-line. This asymmetry corresponds to the nuclear polarization enhancement of 10^3 from the thermal equilibrium value of the polarization at $T = 6.9$ K. Recently, van Tol *et al* reported very similar results at 3 K and 8.58 T [24].

In order to confirm the applicability of a ^{31}P nuclear spin in Si:P as a qubit of the quantum computer of Kane's architecture, investigation of the nuclear spin state of the isolated donor by NMR experiment is needed. Up to now, it has been difficult to observe the NMR signal directly because the P concentration making isolated donors is too low. However, if the nuclear polarization is enhanced by three orders of magnitude over the thermal equilibrium value by the DNP, direct observation of the NMR signal may be possible.

6. Conclusions

A high-frequency steady-state ESR experiment of the donor electron spin in Si:P with $n = 6.5 \times 10^{16}$ cm^{-3} was performed at a high magnetic field of 2.87 T and low temperatures from 1.8 to 45 K with external field modulation. In conjunction with the ESR experiments for Si:P at a similar temperature and in higher field (8.5 T) [25] that have recently been reported, our work provides information on the spin dynamics of an isolated P donor in a silicon crystal at low temperature and in a high magnetic field. The ESR line shape and intensity of Si:P changes drastically with temperature. We could understand that this is due to the fact that T_1 is strongly dependent on temperature and the passage condition changes accordingly. The numerical solutions of the Bloch equations under various passage conditions well explain the experimental data. The relaxation rate obtained from the comparison of the experimental data and numerical calculation is quite consistent with the phonon process that is strongly field dependent. The intensity asymmetry in the hyperfine-split ESR peaks is a new indication of the DNP effect in Si:P. To realize the highly polarized nuclear spins by DNP and observe the NMR signal from the nuclear spins of isolated donors remains for future work.

Acknowledgments

We thank Mr K Sugiyama and Mr K Tanaka at the Graduate School of Engineering, University of Fukui for collaboration in performing the ESR experiment. This work was supported by the Joint Research Project under the Japan–Korea Scientific Cooperation Program, and by the Joint Research Program of the Research Center for Development of the Far-Infrared Region, University of Fukui, and by the National Research Foundation of Korea (NRF) grant funded by the Korean government (MEST) (No. 2009-0078342) and (KRF-2008-313-c00290).

References

[1] Kane B E 1998 *Nature* **393** 133
[2] Jeong M, Song M, Ueno T, Mizusaki T, Matsubara A and Lee S 2009 *J. Phys. Soc. Japan* **78** 075003
[3] Jeong M, Song M, Ueno T, Mizusaki T, Matsubara A and Lee S 2010 *J. Low. Temp. Phys.* **158** 659
[4] Feher G and Gere E A 1959 *Phys. Rev.* **114** 1245
[5] Castner T G Jr 1963 *Phys. Rev.* **130** 58
[6] Song M, Jeong M, Ueno T, Kang B, Sugiyama K, Tanaka K, Matsubara A, Lee S, Mitsudo S, Mizusaki T and Chiba M 2009 *J. Phys.: Conf. Ser.* **150** 022078
[7] Fletcher R C, Yager W A, Pearson G L, Hilden A L, Read W T and Merritt F R 1954 *Phys. Rev.* **94** 1392
[8] Abragam A 1961 *Principles of Nuclear Magnetism* (New York: Oxford University Press) chapter X section IV
[9] Maekawa S and Kinoshita N 1965 *J. Phys. Soc. Japan* **20** 1447
[10] Feher G 1959 *Phys. Rev.* **114** 1219
[11] Portis A M 1956 *Phys. Rev.* **100** 1219
[12] Weger M 1960 *Bell Syst. Tech. J.* **34** 1013
[13] Chiba M, Mitsudo S, Sugiyama K, Ueno T, Mizusaki T, Song M, Kang B, Jeong M and Lee S 2008 *University of Fukui Repository* **9** 127
[14] Chiba M and Hirai A 1972 *J. Phys. Soc. Japan* **33** 730
[15] Tyryshkin A M, Lyon S A, Astashkin A V and Raitsimring A M 2003 *Phys. Rev.* B **68** 193207
[16] Pines D, Bardeen J and Slichter C P 1957 *Phys. Rev.* **106** 489
[17] Orbach R 1961 *Proc. Phys. Soc.* **77** 821
[18] Kohn W and Luttinger M 1955 *Phys. Rev.* **97** 1721
[19] Castner T G Jr 1962 *Phys. Rev. Lett.* **8** 13
[20] Feher G 1956 *Phys. Rev.* **103** 500
[21] Feher G and Gere E A 1956 *Phys. Rev.* **103** 501
[22] Morigaki K and Rosso M 1975 *J. Physique* **36** 1131
[23] McCamey D R, van Tol J, Morley G W and Boehme C 2009 *Phys. Rev. Lett.* **102** 027601
[24] van Tol J, Morley G W, Takahashi S, McCamey D R, Boehme C and Zvanut M E 2009 *Appl. Magn. Reson.* **36** 259
[25] Morley G W, McCamey D R, Seipel H A, Brunel L-C, van Tol J and Boehme C 2008 *Phys. Rev. Lett.* **101** 207602